COMPUTATIONALLY EFFICIENT ANALYSIS OF MICROWAVE INJECTION-LOCKED AMPLIFIERS

Enrico F. Calandra, Marco Caruso and Daniele Lupo
Dipartimento di Ingegneria Elettrica, Elettronica e delle Telecomunicazioni
Ed. 9, Viale delle Scienze, Università di Palermo, Palermo, 90128, Italy

Abstract — In this paper, some preliminary results on a novel approach to the analysis of injection-locked amplifiers are presented. The proposed method is based on a behavioral block modeling of the circuit in the fundamental-frequency dynamical phasor domain. The first-order exact perturbation-refined treatment developed provides, in the end, explicit equations describing the entrained oscillation amplitude and phase dynamics. A secondary simplification then can be adopted in case of low-level injection, to determine a closed form expression for the locking bandwidth, generalizing the well known Adler's one. By virtue of its semi-analytical nature, the proposed approach turns out to be much more efficient and less time consuming, for any design and optimization purpose, with respect to the use of conventional circuit simulators, even those operating in the frequency- and not in the time-domain.

I. Introduction

Injection of a signal of proper amplitude and frequency into an oscillator causes the well know phase-locking phenomenon to occur, which is the basis for several practical applications, mostly in the RF, microwave, millimeter-wave and optoelectronic fields [1-3]. When operated in the so-called fundamental-frequency mode (i.e., with an input signal carrier frequency nearby the oscillator's free-running one) such circuits behave as oscillating amplifiers, and are commonly denominated as injection-locked amplifiers (ILA). They can be effectively adopted as highly-saturated amplifiers for constant-envelope applications or as high-power monochromatic signal sources with excellent phase noise performances [1]. The possibility of simple electronic phase-shifting of the output signal with respect to the reference one, makes them also useful for the beam-steering of phased arrays [2].

In all cases, the two main characterizing specs of an ILA are the injection-ratio ρ, defined as the ratio between the output power of the ILA and the injection signal power (i.e., the equivalent of the power gain for conventional, non-saturated, amplifiers), and the locking bandwidth (LBW) achievable for any given injection-ratio value. Unfortunately, such two quantities are conflicting each-other (a high value of ρ implies a small LBW, and vice versa) and appropriate trade-off has usually to be determined for fulfillment of system-level induced specifications on the ILA.

Initially, the typical design of an ILA was made by modifying an already existing oscillator with the addition of the circuit elements needed for input signal injection and output signal extraction. In the microwave range, this goal was typically achieved by connecting the output of a negative resistance diode oscillator (Gunn, IMPATT, etc.) to the bi-directional interaction port of a non-reciprocal three-port (usually a ferrite circulator), as depicted in Fig.1a. This topological structure of an ILA is usually referred to as "reflection-type". The pro of this configuration is that the oscillator can be designed standalone, through conventional techniques (or an already built oscillator can be "upgraded" to become an ILA). The con is that the injection efficiency is very low and the achievable LBW is consequently very small, at least for reasonable values of the injection ratio. This can make the ILA unattractive even for the narrow band applications in which it is commonly adopted. More recently, with the pervasive adoption of transistors for most low- and medium-power applications (also in the higher microwave range) the situation changed, and the presence of separate input and output ports has permitted to adopt new, more efficient, circuit structures. In this case, the ILA is designed as a whole, incorporating the injection signal mechanism into the oscillation one, in circuit configurations usually referred to as "transmission-type" ILA (TILA, in what follows) [3], as schematically depicted in Fig.1 b.

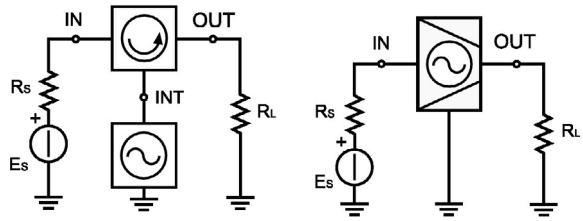

Fig. 1. Reflection-type ILA (a), transmission-type ILA (b)

Appropriately exploited, the degrees of freedom achieved a permit to obtain much better performances for the TILA, especially in terms of band widening. On the other hand, the design phase is more complicated, especially when the more flexible feedback-type topologies (FTILA) are adopted in place of the more conventional negative-resistance ones, with a structure which can often be cast in the general block-diagram illustrated in Fig. 2.

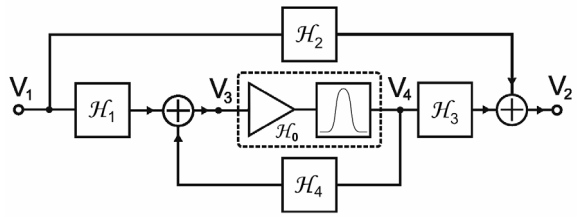

Fig. 2. General block-diagram of the FTILA class analyzed

In this regard, it has to be noted that, for a truly optimized design of ILA's with innovative topologies, the circuit dimensioning problem can became a hard one. Indeed, the typical nowadays design approach, involving repeated circuit simulations in an iterative loop (often based on numerical optimization algorithms), is not well suited for this case. Because of the stiffly-nonlinear nature of the problem at hand, the calculation of ILA performances (notably, the LBW) are extremely time-consuming and not easily automatable, even if most advanced ECAD software is adopted. In fact, the intrinsic slowness of the locking phenomenon, makes impractical all time-domain simulation techniques and anyhow slow also the use of the faster, frequency-domain, numerical transient-envelope based ones.

2011 21st Int. Crimean Conference "Microwave & Telecommunication Technology" (CriMiCo'2011). 12-16 September, Sevastopol, Crimea, Ukraine
 ISBN: 978-966-335-351-7. IEEE Catalog Number: CFP11788

To solve this design-oriented analysis problem, it is proposed here a novel approach in the fundamental-frequency dynamical phasor domain which, because of its semi-analytical nature, can permit evaluation of all FTILA performances in a fraction of time with respect to all other approaches, without limiting the range of applicability to overly simplified circuit topologies or models, as elsewhere proposed.

II. Phasor-Domain Circuit Equations

The starting point of our analysis is the block-diagram illustrated in Fig. 2, representing the general class of FTILA circuits that can be dealt with, after appropriate association of the various blocks to the actual circuit elements. All of its blocks are assumed to be described in the fundamental-frequency dynamical phasor domain, following the theory co-developed by one of these authors in [4]. Of course, this implies that the circuit elements making the "core-oscillator" (blocks $\mathcal{H}_0$ and $\mathcal{H}_4$) are appropriately dimensioned to guarantee that the undriven operation will be that of a high spectral purity quasi-sinusoidal oscillator, as obviously required in any good ILA design. Such high selectivity properties of the center-frequency determining passive filter (here placed inside the main forward gain block $\mathcal{H}_0$), together with the assumption that all the other elements, instead, are relatively wide-band, constitute the only requirement needed to apply - appropriately extended to the two-port nonlinear active device here considered - the basic methods of the cited theory [4]. If we consider that the blocks $\{\mathcal{H}_1\text{-}\mathcal{H}_4\}$ represent passive structures, their frequency-domain transfer functions $\{\mathbf{H}_n=H_n(\omega)\cdot e^{j\phi_n(\omega)},\ n=1,2,3,4\}$ can be easily derived from relevant scattering parameters. This can make their characterization very accurate also in the higher microwave range because of the possibility of adopting, in a combined manner, both circuit and electro-magnetic ECAD simulators and/or experimental measurements. As to the forward gain block $\mathcal{H}_0$, comprising the core-amplifier and filter, the starting point of its dynamical phasor domain modeling (as demonstrated later on) can be a standard Harmonic Balance simulation or, in case of an experiment-based design approach, also a set of X-parameters measurements, to obtain its fundamental-frequency describing function under swept-amplitude sinusoidal-input drive (SIDF) [5].

According to the above considerations, we can now derive a first-approximation exact nonlinear dynamical model of the TILA with the feedback block structure illustrated in Fig.2, under fundamental-mode CW drive.

The first step is to observe that, while the voltage and current at the output port of the core-amplifier could exhibit a significant harmonic content (since working deeply into gain compression) the output of the filter will anyhow be quasi-sinusoidal because of its assumed high-Q. Thus, both voltages at nodes 3 and 4 (as well as those at nodes 1 and 2) can be first-order approximated as quasi-sinusoidal quasi-static ones under transient operation, and characterized by (slowly-varying) phasors $\{\mathbf{V}_n=V_n(t)\cdot e^{j\theta_n(t)},\ n=1,2,3,4\}$. Moreover, if the intrinsic (not filtered) amplifier bandwidth is dimensioned, as reasonable, to be much wider than the filter's one, the selectivity characteristics of this latter will dominate. However, it has to be noted that the assumed presence of a transistor as active device can (and usually does) cause the selectivity characteristics of the filtered amplifier to be function of the drive signal amplitude V_3, because of the nonlinear dependence of the device's output current on both input and output control voltages. Accounting for this phenomenon in a correct manner is a key point of the proposed method, since it constitutes the only way to obtain numerically accurate results. Investigation has shown that, to achieve such accuracy goal, a two-sinusoidal input describing function (TSIDF) [5] can be conveniently adopted for the modeling of the active device nonlinear transconductance. Combining it with a behavioral modeling of the filter, provides the way to generate the overall, reduced order, dynamical model of the filtered amplifier block $\mathcal{H}_0$. Assuming, as usual in this context, a second order ("single-tuned like") model for the resonator, the general expression of the overall SIDF under CW operation, $\mathbf{H}_0(V_3, \omega)$, can be shown to be expressible in the form:

$$\mathbf{H}_0(V_3,\omega)\equiv\frac{\mathbf{V}_4}{\mathbf{V}_3}=\frac{\omega_0(V_3)\cdot A_0(V_3)\cdot e^{j\phi_0}}{\omega_0(V_3)+j2Q_0(V_3)\cdot[\omega-\omega_0(V_3)]},\quad(1)$$

where it has been evidenced that not only A_0, but also ω_0 and Q_0 are taken as functions of V_3. Notice that while the dependence of ω_0 on V_3 is usually numerically negligible, the same is not true for Q_0 (see, e.g., Fig.5 of the example section, and note the group delay variation with V_3). Such fact explains the increased accuracy of this treatment with respect to previous ones, in which $Q_0(V_3)$ is assumed constant and equal to the "small-signal" value $Q_{00}\equiv Q_0(V_3=0)$, i.e., the loaded quality factor of the overall linearized circuit [6-7].

On the basis of above assumptions, it can now be demonstrated that the fundamental-frequency differential relationship between the dynamical phasors $\mathbf{V}_3(t)$ and $\mathbf{V}_4(t)$ can be derived from (1) by making use of the band-limited differential operator (BLDO) concept introduced in [4] for the case of one-port active device ILA's. After some perturbation-refined calculation, this procedure transforms the algebraic equation (1) into its differential counterpart:

$$\left[\omega_0+j2Q_0(\omega-\omega_0-jD)\right]\cdot\mathbf{V}_4(t)=\omega_0\cdot\mathbf{A}_0\cdot\mathbf{V}_3(t),\quad(2)$$

in which $\mathbf{A}_0\equiv A_0(V_3)\cdot e^{j\phi_0}$, "D" stands for the symbolic differentiation operator d/dt, and the dependence on V_3 of A_0, ω_0 and Q_0 has been omitted for compactness. If we combine now (2) with the equation defining V_3:

$$\mathbf{V}_3=\mathbf{H}_1\cdot\mathbf{V}_1+\mathbf{H}_4\cdot\mathbf{V}_4,\quad(3)$$

after some manipulation, we get:

$$\left[\omega_0\cdot(1-\mathbf{A}_0\cdot\mathbf{H}_4)+j2Q_0(\omega-\omega_0)+2Q_0D\right]\cdot V_4\cdot e^{j\theta_4}=$$
$$=(\omega_0\cdot\mathbf{A}_0\cdot\mathbf{H}_1)\cdot V_1\cdot e^{j\theta_1},\quad(4)$$

where the dependence on t has been omitted from V_4 and θ_4, for the sake of brevity.

Expanding derivatives, separating real and imaginary parts and truncating to first-order, we eventually obtain:

$$DV_4=\frac{\omega_0}{2Q_0}\mathrm{Re}\left\{(\mathbf{H}_4+\mathbf{H}_1\frac{V_1}{V_4})\cdot\mathbf{A}_0-1\right\}\cdot V_4\quad(5a)$$

$$D\theta_4=\omega_0-\omega+\frac{\omega_0}{2Q_0}\mathrm{Im}\left\{(\mathbf{H}_4+\mathbf{H}_1\frac{V_1}{V_4})\cdot\mathbf{A}_0\right\},\quad(5b)$$

where θ_1 (the reference phase) has been set to zero.

Equations (3) and (5), together with the output port voltage defining equation:

$$\mathbf{V}_2=\mathbf{H}_2\cdot\mathbf{V}_1+\mathbf{H}_3\cdot\mathbf{V}_4,\quad(6)$$

constitute the first-approximation-exact phasor-domain dynamical model of the FTILA under examination.

2011 21st Int. Crimean Conference "Microwave & Telecommunication Technology" (CriMiCo'2011). 12-16 September, Sevastopol, Crimea, Ukraine
 ISBN: 978-966-335-351-7. IEEE Catalog Number: CFP11788

From this set of equations, both steady-state and transient responses of the FTILA can be evaluated with very high computational efficiency, via standard numerical integration methods. Moreover, calculation of the Jacobian matrix associated to (5) permits evaluation of the dynamical stability of the entrained oscillation under CW injection, leading to accurate and fast calculation of the LBW under any operating condition. If we limit to low-level (LL) injection operation and to a non-selective injection block (i.e., $H_1(\omega)$ nearly constant within the band), a secondary simplification can be adopted to derive a simple, closed-form equation for the LBW (in Hz):

$$LBW_{LL} = \frac{H_1 \cdot V_1 \cdot f_{0,osc}}{Q_{0,osc} \cdot V_{3,osc}}, \qquad (7)$$

in which $Q_{0,osc} \equiv Q_0(V_{3,osc})$ and $f_{0,osc} \equiv f_0(V_{3,osc})$, and where $V_{3,osc}$ represents the steady-state amplitude of V_3 when the oscillator is operating under free-running conditions (i.e., at $V_1=0$ and $\omega=\omega_{0,osc}$), as defined by the solution of the algebraic nonlinear set of equations in $\{V_3, \omega\}$, obtained from (5) setting $DV_4=D\theta_4=V_1=0$:

$$\mathrm{Re}\left\{\mathbf{H}_4(\omega)\cdot\mathbf{A}_0(V_3,\omega)\right\}=1, \qquad (8a)$$

$$\mathrm{Im}\left\{\mathbf{H}_4(\omega)\cdot\mathbf{A}_0(V_3,\omega)\right\}=2Q_0(V_3)\frac{\omega-\omega_0(V_3)}{\omega_0(V_3)}. \qquad (8b)$$

Equation (7) can be interpreted as a generalization of the original Adler's equation [6] and its later extensions [7] to the more complex nonlinear circuit structure here considered and constitutes a main result of our work. Aside from the presence of the quantity H_1, the use of $Q_{0,osc}$ in place of Q_{00} has to be remarked. Notice that such quantity can be straightforwardly determined from the phase slope of $\mathbf{H}_0(V_3, \omega)$ evaluated at $\{V_{3,osc}, \omega_{0,osc}\}$ using a conventional Harmonic Balance simulator.

III. Example of Method's Application

The initial motivation for the development of the presented theory was to have at one's disposal a design-oriented analysis method to be adopted for the correct dimensioning of a microwave FTILA with a novel circuit structure which made no use of nonreciprocal input elements. A prototype of this configuration operating at 10.75GHz was designed and built, and the results presented in [8]. This feedback-type TILA is adopted here also to illustrate the application of the proposed method and to highlight some design and simulation aspects previously not presented. The structure of the circuit realized is illustrated in Fig.3.

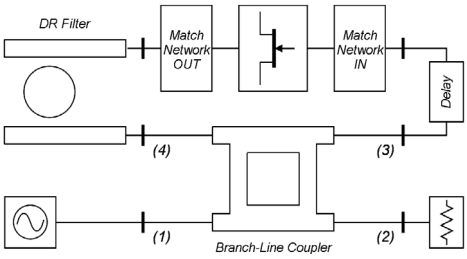

Fig. 3. Circuit-diagram of the X-band example FTILA

There are evidenced: the (50Ω matched) 3dB hybrid Branch-Line Coupler (BLC) committed to the coupling of the in/out power, the delay line feeding the transistor amplifier, and the Dielectric Resonator transmission-type filter closing the loop. The microwave amplifier was made using a single PHEMT device (ATF-36077), out-of-band stabilized and input matched to 50Ω (under large signal operation). The output matching network was designed to provide reasonable gain under small signal operation and full power under large signal operation into 50Ω. The DR filter was dimensioned using advanced EM simulation tools after having determined its specs on the basis of the results of the application of the proposed method. Further details on the TILA prototype can be found in [8].

During the design phase of such TILA, the theory presented in previous section was adopted cyclically for the initial dimensioning and subsequent refining of the DR filter and delay line structures to satisfy project specifications. This procedure was greatly simplified by the semi-analytic nature of the method which permits to enucleate critical design parameters and use them for their approximate direct dimensioning. For the purpose of this presentation we skip over the details of this nested design loops and focus mainly on the analysis method application. To this end, we can refer to the TILA simplified behavioral macro-model shown in Fig. 4, which closely relates to the general diagram of Fig. 2, once the four blocks $\{\mathcal{H}_1\text{-}\mathcal{H}_4\}$ are associated to BLC and the $\mathcal{H}_0$ block to the remaining circuit elements.

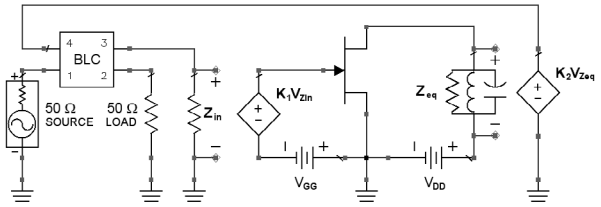

Fig. 4. Macro-model of the example FTILA analyzed

In Fig. 4 the equivalent RLC parallel resonator models the resonant impedance Z_{eq} associated to the DR filter, as seen by the "intrinsic" transistor, described as a memoryless nonlinear 2D-VCCS element. All the remaining parasitic elements and losses/delays are absorbed (as amplitude and phase of the coefficients $\mathbf{K}_1$ and $\mathbf{K}_2$) into the two VCVS's which model the stages preceding and following the transistor. Though not evident from the figure, in our case Z_{in}, i.e. the amplifier large-signal input impedance, was dimensioned to 50Ω, for modularity purposes. To achieve the desired locking bandwidth for the nominal value (-20dBm) of the injection signal, in view of (7), one has to obtain the correct value of the product $Q_{0,osc} \cdot V_{3,osc}$ acting on the free design parameter set. In our specific design we selected the insertion losses and the loaded Q-factor of the DR filter block, which, together with the constraint set on its in/out 50Ω match, determines the position and the distance of the DR puck with respect to the two coupled microstrip lines. In our model this induces a parametric dependence of $\mathbf{K}_2$ and Q_{00} on filter geometry. As previously remarked, knowing Q_{00} does not suffice to compute $Q_{0,osc}$, and thus evaluate LBW_{LL}. Therefore, even if a global, parametric, analytical or numerical model of all components (e.g., the DR filter) is available, a few design iterations are still required to achieve the targeted value of LBW_{LL}. The situation corresponding to our final design is depicted by Figs. 5-6. In Fig. 5 the dependence of amplitude and phase of $\mathbf{H}_0$ on drive voltage V_3 and frequency detuning $\Delta f=(f-f_{0,osc})$ is illustrated. Notice that the amplitude of the free-running oscillation $V_{3,osc}$ is around 0.176 [V], and corresponds to $H_0 \approx 1.5$, leaving around +5dB as gain margin for a robust oscillation buildup. The final value of the RLC Q-factor is ≈480, which corresponds to a loaded Q-factor of the linearized circuit of ≈435 (Q_{00} in our terminology), which further re-

 ISBN: 978-966-335-351-7. IEEE Catalog Number: CFP11788

duces, because of the nonlinear effects here accounted for, to ≈300 ($Q_{0,osc}$ in our terminology), i.e., 30% less than predicted by current theories adopting Adler's equation [7]. Such improvement in accuracy is clearly seen in the graph of Fig.6, which compares the measured locking bandwidth with the simulated ones obtained adopting our formula (7) or the classical one. A good agreement between prediction and experiments can be observed only in the first case. In this regard, it can be noticed that to achieve analogous accuracy in the locking bandwidth prediction, the only alternative is to adopt a transient envelope numerical simulation tool, such as the "Circuit Envelope" option of the Advanced Design System by Agilent-EEsof [9]. However, a number of repeated simulations are required to determine, by bracketing stable and unstable points, the band limit to within a reasonably tight tolerance. Furthermore, each one of these searches involves a long transient, even in a stroboscopic time scale. Summing up, this latter method, while much faster of brute force time-domain simulations, remains orders of magnitude more time consuming than the proposed one.

IV. Conclusions

In this work, a novel approach to the computationally efficient simulation of feedback transmission-type oscillating amplifiers (FTILAs) was presented. In a first step, the elements of the block model of the system are identified in the frequency domain, using standard linear or Harmonic Balance simulation methods. The extended BLDO associated to the amplifier-filter block can thus be derived, if necessary, after a preliminary analysis of the free-running regime. Closed form expressions are finally derived for the state equations defining the entrained oscillator dynamics. Numerical methods can then be adopted to calculate, with very high computational efficiency, all properties of the locked oscillator in a first-order exact manner (from a perturbation point of view).

Using a secondary simplification, valid for a low-level operation (i.e., high values of the injection ratio ρ), as typical of most practical applications, a closed-form expression for the LBW has been also presented, which generalizes the Adler's formula.

It can be remarked that all quantities characterizing the dynamical model of the FTILA can be obtained either analytically (in simpler cases) or via standard frequency-domain circuit simulators (linear or Harmonic Balance based). In the higher frequency range, electro-magnetic simulation tools can also be advantageously resorted to for increased accuracy. In any case, the computational effort involved in this modeling phase is very limited. In case of low-level injection the only "nonlinear" parameter to be evaluated is $Q_{0,osc}$, which can be calculated from the phase slope of the nonlinear transfer function of the filtered amplifier block obtained via CW-HB simulation.

The example of method application presented has shown that, also in those cases in which Adler theory would become imprecise, very accurate results can be achieved by the proposed approach, at a fraction of time of what would be required using even the most advanced ECAD software tools available in the market. Therefore, this approach looks promising for the purpose of optimal design oriented practical applications.

V. References

[1] *Kurokawa K.* Injection locking of microwave solid-state oscillators // Proc. of the IEEE. 1973. Vol. 61. P. 1386—1410.

[2] *Phase* control of optically injection locked oscillators for phased arrays / A. Daryoush, et al. // IEEE MTT-S International Microwave Symposium Digest (8—10 May 1990). P. 1247—1250.

[3] *Tajima Y., Mishima K.* Transmission-type injection locking of GaAs Schottky-barrier FET oscillators // IEEE Trans. Microwave Theory Tech. 1979. Vol. 27. P. 386—391.

[4] *Calandra E. F., Sommariva A.* Approach to the analysis of nonlinear feedback oscillators under large-signal injection // IEE Proc. 1986. Vol. 133, Pt. G, No. 5. P. 233—241.

[5] *Gelb A., Vander Velde W. E.* Multiple-Input Describing Functions and Nonlinear System Design. McGraw Hill, 1968.

[6] *Adler R.* A study of locking phenomena in oscillators // Proc. IRE, 34 (June 1946). Reprinted in Proc. IEEE, 61:10, 1973. P. 1380—1385.

[7] *Ohira T.* Extended Adler's injection locked Q factor formula for general one- and two-port active device oscillators // IEICE Electronics Express. 2010. Vol. 7, No. 19. P. 1486—1492.

[8] *Calandra E., Lupo D., Puccio L.* A DRO-based X-band Injection-Locked Amplifier Without Input Non-reciprocal Elements // Proc. of ECCTD Conference (Antalya, Aug. 2009). 2009. P. 367—370.

[9] *Agilent-EEsof:* Advanced Design System 2009. User Guide.

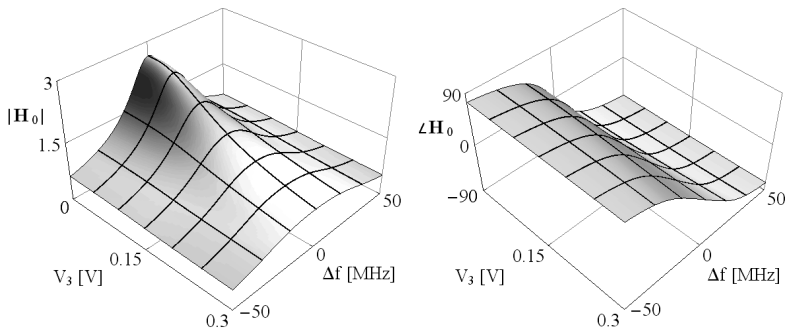

Fig. 5. 3D plots $\boldsymbol{H}_0$ as function of drive voltage V_3 and of frequency detuning $\Delta f = (f-f_{0,osc})$: magnitude (left) and phase (right)

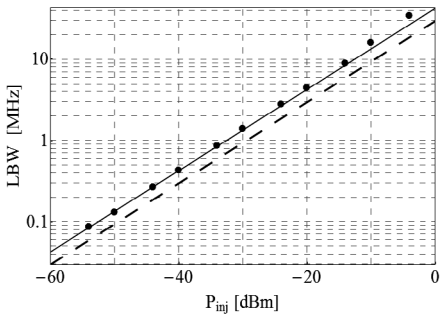

Fig. 6. Comparison of LBW's for the example FTILA: this theory (solid line), (dashed line), Adler's formula measurements (dots)

2011 21st Int. Crimean Conference "Microwave & Telecommunication Technology" (CriMiCo'2011). 12-16 September, Sevastopol, Crimea, Ukraine
 ISBN: 978-966-335-351-7. IEEE Catalog Number: CFP11788